Numerical modelling of stainless steel bolted T-stubs in tension

Orhan Yapici [1*], Marios Theofanous [2], Sheida Afshan[3], Huanxin Yuan[4], Samir Dirar[2]

[1] *Institute for Infrastructure & Environment, Heriot-Watt University, Edinburgh, EH14 4AS, United Kingdom*

[2] *Department of Civil Engineering, University of Birmingham, Birmingham, B15 2TT, United Kingdom*

[3] *Faculty of Engineering and Physical Sciences, University of Southampton, Southampton SO16 7QF, United Kingdom*

[4] *School of Civil Engineering, Wuhan University, Wuhan 430072, PR China*

[*]corresponding author:

Orhan Yapici, Institute for Infrastructure & Environment, Heriot-Watt University, Email: o.yapici@hw.ac.uk

Abstract

Recently, a series of experimental tests and accompanying numerical studies has been conducted on austenitic and duplex stainless steel moment resisting connections which highlighted both the excellent ductility and significant overstrength exhibited by such connections as well as the severe conservatism of current design rules specified in EN 1993-1-8 when applied to stainless steel joints. This study builds upon a previous experimental research on bolted austenitic and duplex stainless steel T-stubs in tension conducted by the authors and reports in depth the development and validation of an advanced FE model able to predict the overall behaviour, failure modes and fracture mechanisms of bolted T-stubs in tension. Key simulation strategies regarding the explicit modelling of bolt geometry and overcoming numerical instabilities are discussed and recommendations on best modelling practices are made. The model is utilised thereafter to conduct parametric studies on austenitic, duplex and ferritic stainless steel T-stubs of various geometric configurations, thus investigating the effect of plate thickness, material grade, bolt spacing and bolt strength on the joint plastic resistance, ultimate capacity, ductility as well as overall response. Based on the obtained results, the design provisions of EN 1993-1-8 are assessed.

Keywords: Stainless steel, T-stub, Bolted connections, Tension resistance, Numerical modelling, Connections, Stainless steel joints.

1. Introduction

To determine the strength and stiffness of bolted beam-to-column connections, EN 1993-1-8 [1] utilises a semi-analytical design framework called the component method, according to which the overall joint response can be assembled from the response of individual joint components comprising the connection. To this end, moment resisting connections are divided into three main regions according to the forces they are subjected to, namely the tension zone, the compression zone and the shear zone. For each zone, the basic components contributing to its strength and stiffness are identified and the strength and stiffness of each component is evaluated according to codified design expressions [1].

Among all components idealising the tension zone of bolted moment resisting connections, the equivalent T-stub, pioneered by Zoetemeijer [2], is widely used to idealise the behaviour of the column flange and end plate in bending [2-8]. In most cases the strength of the equivalent T-stub limits the strength of the tension zone and hence the moment resistance of the overall connection whilst also being the least stiff component. Therefore, the behaviour of T-stubs has been extensively studied both experimentally [9-11] and analytically [12-16], resulting in several simplified approaches for the determination of the post yield behaviour of the T-stubs in order to obtain its ultimate response [10-16]. Additionally, numerous FE models for steel T-stubs have been reported in the literature [17-28].

Most of the published research on the behaviour of connections and equivalent T-stubs in tension exclusively focuses on carbon joints, whilst similar studies on the behaviour of stainless steel connections and isolated T-stubs remain scarce in comparison. The first numerical results on the ductility and ultimate behaviour of stainless steel bolted T-stubs were reported by

Bouchaïr et al. [29], who highlighted the significant conservativism of the design predictions of EN 1993-1-8 [1] due to the pronounced strain-hardening of stainless steel. Yuan et al. [30] reported the first experimental study on austenitic and duplex stainless steel bolted T-stubs under tension, which confirmed the significant conservatism of the design predictions of international design codes. This study was complemented by the first systematic experimental and numerical studies on full-scale stainless steel beam-to-column joints, the failure of which was governed by the failure of equivalent T-stubs [31-33] and similar conclusions were reached. Additional studies on stainless steel connections were reported by Wang et al. [34], Bu et al. [35], Song et al. [36], Gao et al. [37], Yuan et al. [38] and Yapici et al. [39-41] conducted experimental and numerical studies on the behaviour of stainless steel connections and reported similar conclusions.

In this study, an advanced FE model which is able to predict the overall behaviour, failure modes and ultimate load of stainless steel bolted T-stubs in tension was developed and validated against available experimental data reported by Yuan et al. [30] on stainless steel bolted T-stubs. Different simulation approaches regarding the modelling of bolt geometry are reported and relevant recommendations are made. Upon validation of the proposed model, a parametric study is performed for various geometric configurations thus enabling the effect of governing parameters such as plate thickness, material grade, bolt spacing and bolt strength on the joint plastic resistance, ultimate capacity, ductility as well as overall response to be quantified. Finally, the design provisions of EN 1993-1-8 [1] are assessed based on the obtained results.

2. Development of FE model

2.1 Modelling assumptions

The geometric configurations of the specimens tested by Yuan et al. [30] are defined in Table 1 and Fig. 1 for single-row and double-row T-stub connections. These tests are numerically replicated herein.

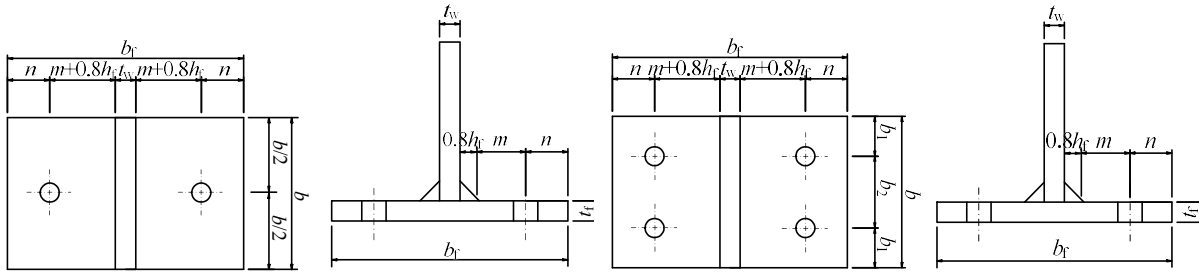

(a) T-S (b) T-D

Fig. 1. Geometric properties of a) single and b) double bolt rows T-stub specimens [30].

The T-stub specimens were manufactured by welding two hot-rolled stainless steel plates to one another. Two nominal plate thicknesses (8 mm and 12 mm), two different bolt diameters (12 mm and 16 mm) and two different bolt configurations (single bolt row TS-S and double bolt row TS-D) with various bolt spacings are considered. It should be noted that a third bolt configuration employing 4 bolts per row was also considered by Yuan et al. [30], but this is beyond the scope of this study. The measured geometric properties of each specimen are summarised in Table 1 in which d_b corresponds to the nominal bolt diameter and h_f is the fillet weld size. Other geometric symbols included in Table 1 are defined in Fig. 1. The fillet weld size h_f is specified as 5 mm and 6 mm for a plate thickness of 8 mm and 12 mm, respectively.

Table 1. Geometric dimensions of T-stub specimens [30]. (All dimensions are in mm)

Type	Specimen	Material	Bolt	d_b	n_1	n_2	n	m	b_1	b_2	b	b_f	$t_f = t_w$	h_f
TS-S	S1	EN 1.4301	A4-70	16	-	-	50	50.2	-	-	120	222	11.85	6
	S2	EN 1.4301	A4-80	12	-	-	35	65.2	-	-	120	222	11.85	6
	S3	EN 1.4462	A4-80	16	-	-	50	50.2	-	-	90	222	12.58	6
	S4	EN 1.4462	A4-80	12	-	-	50	53.0	-	-	120	222	7.72	5
	S5	EN 1.4462	A4-80	16	-	-	50	53.0	-	-	90	222	7.72	5
	S6	EN 1.4301	A4-80	12	-	-	50	53.0	-	-	120	222	7.85	5
	S7	EN 1.4462	A4-80	16	-	-	50	53.0	-	-	120	222	7.72	5
	S8	EN 1.4301	A4-70	16	-	-	50	50.2	-	-	90	222	11.85	6
	S9	EN 1.4301	A4-80	12	-	-	35	65.2	-	-	120	222	11.85	6
TS-D	D1	EN 1.4301	A4-70	16	-	-	50	50.2	40	70	150	222	11.85	6
	D2	EN 1.4301	A4-80	12	-	-	35	65.2	40	70	150	222	11.85	6
	D3	EN 1.4462	A4-70	16	-	-	35	68.0	40	70	150	222	7.72	5
	D4	EN 1.4462	A4-70	16	-	-	35	65.2	40	70	150	222	12.58	6
	D5	EN 1.4462	A4-70	16	-	-	50	50.2	40	70	150	222	12.58	6
	D6	EN 1.4301	A4-80	16	-	-	35	65.2	40	70	150	222	11.85	6
	D7	EN 1.4301	A4-80	12	-	-	35	65.2	28	54	110	222	11.85	6
	D8	EN 1.4301	A4-80	12	-	-	35	65.2	40	70	150	222	11.85	6

Accurate geometric modelling of the specimens may lead to overly high computational cost. The bolts contain a threaded part, which is tedious to model explicitly and necessitates the adoption of a very fine mesh locally to accurately discretise it, as the thickness of the threads is very small [42]. In addition to the high number of elements, modelling the threaded part may also lead to a low stable time increment in quasi-static explicit dynamic analyses, thus further increasing computational time. An additional question relates to the need to explicitly model the weld toe at the flange-to-web junction of the T-stubs, or whether simulating the effect of welding via tying to one another the degrees of freedom of the welded parts over the weld toe region suffices.

To determine an optimal modelling strategy, four types of numerical models with different levels of complexity were considered. In the first model, a cylindrical bolt with an effective diameter such that its cross-sectional area is equal to the nominal stress area of the threaded bolt is used. This approach leads to larger clearance between the bolt and the bolt hole and hence different contact conditions, or to a reduction of the modelled clearance hole diameter, thus assuming the existence of material that is physically not there. In the second model, the diameter of the unthreaded part of the bolt is considered, in order to maintain the same clearance between the bolt and the bolt hole, but material from the central part of the bolt is removed so that its cross-sectional area matches the nominal cross-sectional area of the threaded bolt. The resulting geometry of the bolt is bounded by two concentric cylinders. For each of the two models for the bolt, two variations of modelling the weld toe are considered, one where the weld toe is explicitly modelled with triangular elements and one where it is omitted and only a tie constraint is applied. The generated numerical models are designated as Type-1, Type-2, Type-3 and Type-4, as outlined in Fig. 2.

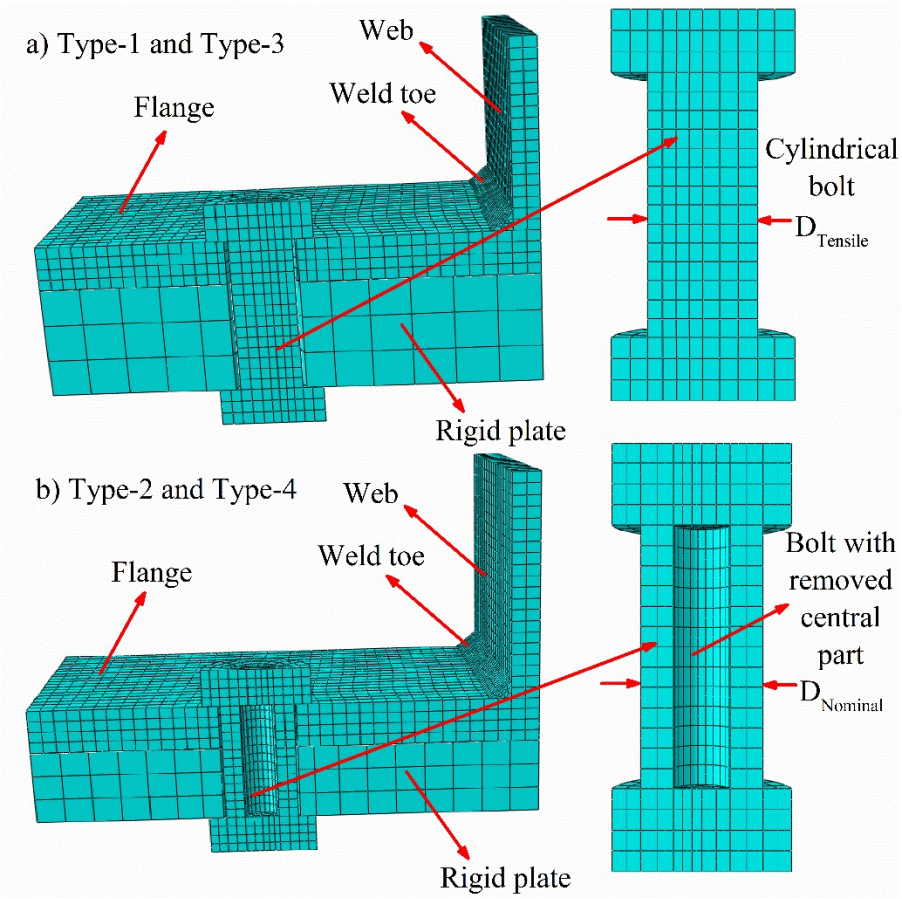

Fig. 2. Geometric modelling assumptions for the bolt and the weld toe.

Three dimensional nonlinear finite element analysis is carried out to determine the ultimate strength and the corresponding displacement of the T-stubs using ABAQUS [43]. To minimise computational time without compromising accuracy, the symmetry of the model in terms of geometry, applied load, boundary conditions and structural response is exploited. Hence, one quarter of the T-stub is modelled and appropriate boundary conditions are applied along the planes of symmetry. In line with the conducted tests, the T-stub models are attached via bolts to a reaction 20 mm thick T-stub, which is discretised with rigid elements with all its degrees of freedom being fixed. Surface to surface contact is defined between bolt shank and bolt hole, bolt head and flange, bolt head and rigid T-stub and T-stub and rigid reaction T-stub. The contact behaviour for each contact pair is assumed hard in the normal direction hence eliminating any penetration and finite sliding with a friction coefficient of 0.25 is assumed in

the tangential direction thus allowing contact conditions to change as the analysis progresses. It is noted that the effect of using different friction coefficients was also investigated but was found to be very small.

To obtain an optimal mesh for the subsequent parametric studies the effect of the employed element type and mesh size on the obtained results was investigated. Both the T-stub and the bolts were discretised with a uniform mesh with a characteristic element size equal to either 1/3 or 1/4 of the flange thickness, as earlier studies [32] showed that at least three linear elements are required through the thickness of a plate in bending to obtain accurate results and avoid shear locking. Moreover, the performance of linear and quadratic elements was compared with the 8-noded reduced integration continuum solid elements C3D8 and the 20-noded reduced integration continuum solid elements C3D20R being employed.

For each of the resulting four meshes (2 element types and 2 mesh sizes) two analysis types were conducted. Initially, a static Riks analysis [43], which is a variant of the classic arc-length method was conducted. It resulted in long computational times and in some cases loss of convergence due to the highly nonlinear nature of the problem involving several contact interactions. To reduce computational time a quasi-static explicit dynamic analysis was also attempted, which can easily handle highly nonlinear problems at a reduced computational cost. For the explicit dynamic analysis, a mass scaling factor of 10^{-4} was adopted to reduce computational time; in all cases it was ensured that the kinetic energy of the model was below 2% of its internal energy thus resulting in a quasi-static response. The results for the 2 analysis types are compared hereafter for each of the 4 geometric modelling strategies employed for the modelling of the bolts and the weld toes, as well as for the different mesh densities and element types considered.

2.2 Material modelling

The material properties of the stainless steel T-stubs and the connecting bolts are adopted from the study conducted by Yuan et al. [30] and are given in Table 2. The standard von Mises yield criterion with isotropic hardening is employed to simulate the plastic behaviour of the T-stubs. The material behaviour beyond the nominal yield stress $\sigma_{0.2}$ is approximated by the 3 stage Ramberg-Osgood expression [44]. All material models are defined in the required true stress-logarithmic plastic strain format, with the highest stress values considered corresponding to the experimentally determined ultimate tensile stress σ_u.

Table 2. Material properties of stainless steel plates and bolts [30]

Stainless steel plates and bolts	Plate thickness or nominal bolt diameter (mm)	v	E_0 (MPa)	$\sigma_{0.01}$ (MPa)	$\sigma_{0.2}$ (MPa)	$\sigma_{1.0}$ (MPa)	σ_u (MPa)	ε_u (%)	ε_f (%)	n
EN 1.4301	7.85	0.257	180700	191.4	291.7	338.9	706.0	-	62.9	7.1
EN 1.4301	11.85	0.258	182800	184.7	280.4	319.1	719.6	-	57.7	7.2
EN 1.4462	7.72	0.207	188700	296.5	551.4	614.5	738.4	19.3	33.0	4.8
EN 1.4462	12.58	0.226	184000	227.8	464.6	552.8	705.3	23.3	37.4	4.2
A4-70	12	-	175400	273.8	522.6	667.1	758.1	8.5	36.5	4.6
A4-70	16	-	173000	283.8	484.6	622.7	732.7	26.0	44.9	5.6
A4-80	12	-	184500	271.5	553.9	710.4	794.0	5.9	29.7	4.2
A4-80	16	-	175300	300.7	524.4	682.3	765.4	9.8	33.4	5.4

3. Results and dıscussıons

3.1 Modelling of bolt and weld toe

For each of the four types of geometric modelling considered for the simulation of the bolt geometry and the weld toe, as defined in Fig. 2, the ultimate resistances and corresponding displacements were obtained from the static Riks analysis are presented in Tables 3-4. Only the models employing linear continuum elements have been considered herein to assess the effect of modelled geometry for the weld toes and bolts on the obtained response. To facilitate a direct comparison with the experimental values, the reported results are normalised by the corresponding experimental ones. As expected, the observed scatter of the numerical over

experimental displacement values is considerably higher than that observed for the ultimate force predictions shown in Tables 3-4, respectively. This is attributed to the high sensitivity of the experimental stiffness on existing imperfections and applied level of bolt pretensioning. Hence, the experimental displacements are less suitable to assess the quality of the numerical results and only ultimate resistance F_u are considered hereafter.

In Table 3, it can be seen that the mean value of the numerical over the experimental ultimate resistance ratio $F_{u,\,FEM}/\ F_{u,\,Exp}$ obtained for type-2 and type-3 models is 1.00 for both mesh densities considered (i.e. with 3 and 4 elements through the flange thickness) with a coefficient of variation (COV) of 0.06 and 0.07, respectively. The mean value of $F_{u,\,FEM}/\ F_{u,\,Exp}$ ratios for the type-4 model were determined as 1.02 and 1.03 for the mesh configurations with 3 and 4 elements. Hence it can be concluded that both mesh densities lead to similar levels of accuracy in terms of the ultimate resistance F_u. The numerical analysis results using four elements through the flange thickness show only slightly lower coefficient of variation values in terms of ultimate force. Overall, it can be concluded that as long as the modelled bolt has a cross-sectional area equal to the effective area of the threaded bolt used in the tests, reasonably accurate results can be obtained. In the remainder of this study all models explicitly include the geometry of the weld (Type-3 and Type-4).

Table 3: Effect of modelling type and number of elements through the flange thickness on ultimate resistance F_u.

		Type-1	Type-2	Type-3	Type-4	Type-1	Type-2	Type-3	Type-4
		3 elements through flange thickness				4 elements through flange thickness			
Specimens	$F_{u,Exp}$ (KN)	$F_{u,FEM}/F_{u,Exp}$	$F_{u,FEM}/F_{u,Exp}$	$F_{u,FEM}/F_{u,Exp}$	$F_{u,FEM}/F_{u,Exp}$	$F_{u,FEM}/F_{u,Exp}$	$F_{u,FEM}/F_{u,Exp}$	$F_{u,FEM}/F_{u,Exp}$	$F_{u,FEM}/F_{u,Exp}$
S1	200.2	0.95	0.95	0.98	0.95	0.95	0.94	0.98	0.96
S2	106.8	0.96	0.94	0.95	1.01	0.98	0.97	0.96	1.02
S3	198.4	0.95	0.96	0.98	0.98	0.96	0.97	1.00	0.98
S4	108.9	0.95	1.02	0.97	1.03	0.95	1.01	0.98	1.03
S5	161.6	1.06	1.04	1.08	1.07	1.04	1.04	1.06	1.07
S6	104.3	0.91	1.00	0.95	1.04	0.95	1.00	0.97	1.04
S7	175.2	0.81	0.87	0.85	0.90	0.80	0.87	0.85	0.90
S8	188	0.99	0.99	1.01	0.99	0.98	0.98	1.00	1.00
S9	108.9	0.94	0.93	0.93	0.99	0.96	0.95	0.94	1.00
D1	367.5	1.01	1.00	1.03	1.02	1.01	0.99	1.02	1.00
D2	179.1	1.00	1.04	1.02	1.06	0.98	1.04	1.00	1.07
D3	260.9	1.11	1.13	1.15	1.16	1.13	1.13	1.14	1.15
D4	312.5	1.06	1.04	1.08	1.07	1.07	1.04	1.06	1.06
D5	382.5	0.94	0.95	0.97	0.98	0.94	0.94	0.97	0.97
D6	306.6	1.05	1.02	1.05	1.04	1.05	1.02	1.07	1.05
D7	174.3	1.00	1.04	1.02	1.06	1.00	1.04	1.03	1.07
D8	181.6	0.99	1.02	1.01	1.05	0.97	1.02	0.99	1.05
Mean		0.98	1.00	1.00	1.02	0.98	1.00	1.00	1.03
COV		0.07	0.06	0.07	0.06	0.07	0.06	0.06	0.05

Table 4: Effect of modelling type and number of elements through the flange thickness on displacement at ultimate resistance Δ_u.

		Type-1	Type-2	Type-3	Type-4	Type-1	Type-2	Type-3	Type-4
		3 elements through flange thickness				4 elements through flange thickness			
Specimens	$\Delta_{u,Exp}$ (mm)	$\Delta_{u,FEM}/\Delta_{u,Exp}$	$\Delta_{u,FEM}/\Delta_{u,Exp}$	$\Delta_{u,FEM}/\Delta_{u,Exp}$	$\Delta_{u,FEM}/\Delta_{u,Exp}$	$\Delta_{u,FEM}/\Delta_{u,Exp}$	$\Delta_{u,FEM}/\Delta_{u,Exp}$	$\Delta_{u,FEM}/\Delta_{u,Exp}$	$\Delta_{u,FEM}/\Delta_{u,Exp}$
S1	31.8	1.214	1.084	1.166	0.975	1.191	1.080	1.174	1.029
S2	23.9	0.788	0.903	0.827	0.823	0.822	0.862	0.843	0.853
S3	21.5	0.978	0.933	0.887	0.871	0.947	0.928	0.887	0.868
S4	19.7	1.040	1.046	0.921	0.968	0.971	1.036	0.901	0.949
S5	29.2	1.284	1.286	1.192	1.233	1.272	1.235	1.172	1.229
S6	26	0.966	0.981	0.947	0.968	1.108	1.089	1.101	0.971
S7	28.9	0.845	0.893	0.838	0.831	0.854	0.867	0.840	0.846
S8	27.3	1.414	1.262	1.358	1.136	1.387	1.258	1.368	1.199
S9	25	0.753	0.863	0.791	0.787	0.786	0.824	0.806	0.815
D1	28.7	1.426	1.392	1.396	1.345	1.537	1.491	1.435	1.422
D2	22.5	1.161	1.050	1.072	1.035	1.108	1.142	1.023	1.049
D3	33.6	1.273	1.365	1.295	1.330	1.368	1.385	1.345	1.355
D4	25.4	1.622	1.545	1.600	1.557	1.724	1.583	1.506	1.552
D5	26	1.181	1.190	1.173	1.111	1.224	1.208	1.159	1.096
D6	31.4	1.280	1.234	1.230	1.247	1.311	1.278	1.297	1.254
D7	25.8	1.165	1.124	1.098	1.076	1.193	1.192	1.177	1.105
D8	25.3	1.032	0.934	0.953	0.921	0.985	1.015	0.910	0.933
Mean		1.144	1.129	1.105	1.076	1.170	1.153	1.112	1.090
COV		0.209	0.184	0.210	0.201	0.226	0.194	0.200	0.200

3.2 Effect of element type

The results obtained from Type-3 and Type-4 models discretised with linear elements are compared to those obtained using quadratic elements to assess the effect of element type on the obtained response. For both element types, two mesh densities were considered as previously discussed. The experimental and numerical force-displacement curves for specimens S4 and D2 are shown in Fig. 3 to demonstrate the effect of the employed element type. The numerical models employing quadratic elements exhibit an almost identical behaviour to that of the models employing linear elements up to the attainment of the ultimate resistance. However, for the models with quadratic elements, it was observed that after the ultimate load was reached, the force drop was sharper.

The comparison of the mean and COV values of the ultimate resistance ratios are given in Table 5. For completeness, the ratios for the corresponding displacements are also given in Table 6. The data considered for these tables are the same as previously (Tables 3-4) but for brevity only the average values and COV of the key response parameters are reported. It can be concluded that the effect of using quadratic elements instead of linear ones on the ultimate force predictions is not significant for accuracy, but significantly increases the computational cost. In terms of ultimate displacements, quadratic elements provide slightly better and more consistent results. Additionally, the Type-3 numerical model using a cylindrical bolt exhibits better results in terms of ultimate force values and it provides simpler and faster solution. Given the simplicity of modelling a cylindrical bolt with an effective diameter, only Type-3 only are considered hereafter and in the parametric studies. Furthermore, due to the close agreement of the response of the models with 3 elements through the flange thickness with the experimental one and the significant savings in computational time, 3 elements through the thickness are adopted.

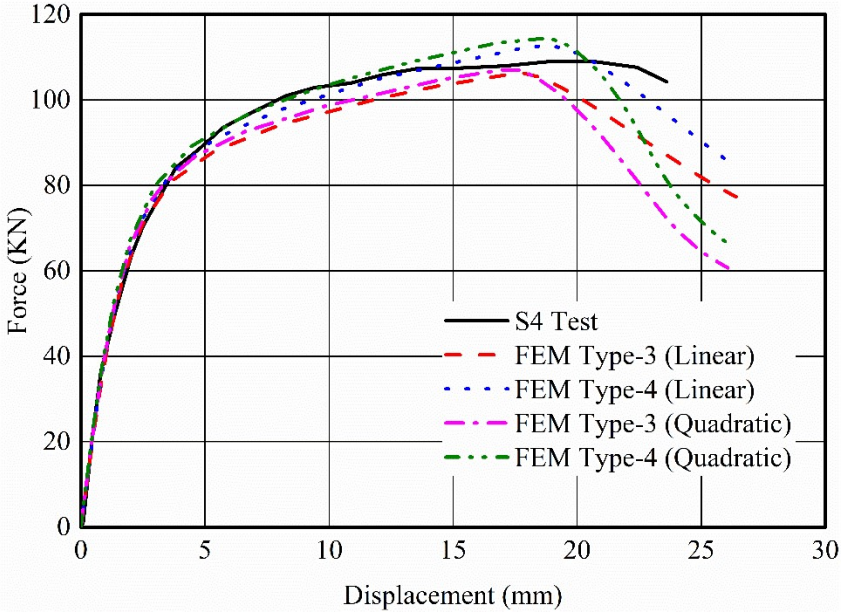

(a)

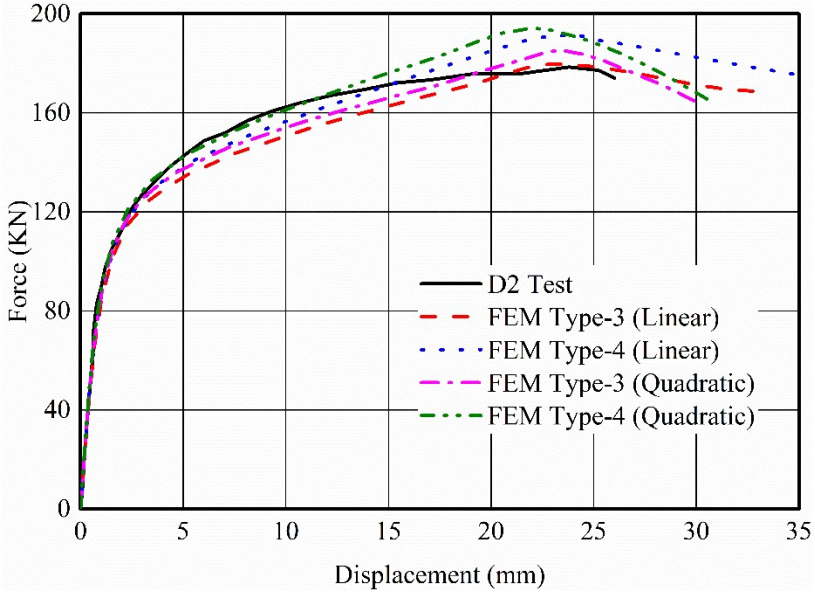

(b)

Fig.3. Force-displacement curves of the a) S4 and b) D2 specimens.

Table 5: Comparison of the mean values of $F_{u,\,FEM}$ / $F_{u,\,Exp}$ ratios for Type-3 and Type-4.

	Type-3				Type-4			
	3 elements through flange thickness		4 elements through flange thickness		3 elements through flange thickness		4 elements through flange thickness	
	Linear mesh	Quadratic mesh	Linear mesh	Quadratic mesh	Linear mesh	Quadratic mesh	Linear mesh	Quadratic mesh
	$F_{u,\,FEM}$/ $F_{u,Exp}$	$F_{u,\,FEM}$/ $F_{u,Exp}$	$F_{u,\,FEM}$/ $F_{u,Exp}$	$F_{u,\,FEM}$/ $F_{u,Exp}$	$F_{u,\,FEM}$/ $F_{u,Exp}$	$F_{u,\,FEM}$/ $F_{u,Exp}$	$F_{u,\,FEM}$/ $F_{u,Exp}$	$F_{u,\,FEM}$/ $F_{u,Exp}$
Mean	1.00	1.01	1.00	1.00	1.02	1.03	1.03	1.03
COV	0.07	0.06	0.06	0.06	0.06	0.05	0.05	0.05

Table 6: Comparison of the mean values of $\Delta_{u,\,FEM}$ / $\Delta_{u,\,Exp}$ ratios for Type-3 and Type-4.

	Type-3				Type-4			
	3 elements through flange thickness		4 elements through flange thickness		3 elements through flange thickness		4 elements through flange thickness	
	Linear mesh	Quadratic mesh	Linear mesh	Quadratic mesh	Linear mesh	Quadratic mesh	Linear mesh	Quadratic mesh
	$\Delta_{u,\,FEM}/\Delta_{u,Exp}$	$\Delta_{u,\,FEM}/\Delta_{u,Exp}$	$\Delta_{u,\,FEM}/\Delta_{u,Exp}$	$\Delta_{u,\,FEM}/\Delta_{u,Exp}$	$\Delta_{u,\,FEM}/\Delta_{u,Exp}$	$\Delta_{u,\,FEM}/\Delta_{u,Exp}$	$\Delta_{u,\,FEM}/\Delta_{u,Exp}$	$\Delta_{u,\,FEM}/\Delta_{u,Exp}$
Mean	1.11	1.08	1.11	1.08	1.08	1.04	1.09	1.04
COV	0.21	0.19	0.20	0.19	0.20	0.18	0.20	0.17

3.3 Effect of analysis type

In this section, the results obtained using the static Riks analysis procedure are compared with those obtained using the quasi-static explicit dynamic analysis. Table 7 summarizes the mean value of the $F_{u,\,FEM}/\,F_{u,\,Exp}$ ratios obtained from a static Riks analysis with 3 linear or 3 quadratic elements through the flange thickness as well as the corresponding results from a quasi-static explicit dynamic analysis with 3 linear elements through the flange thickness. It should be noted that quadratic elements are not supported for explicit analysis [43]. It can be seen that, the mean values of the $F_{u,\,FEM}/\,F_{u,\,Exp}$ ratio for the explicit dynamic analysis was 1.00, which is equal to that of the static Riks analysis with linear elements. Furthermore, the coefficient of variation was for the explicit dynamic analysis was 0.06, slightly lower than the respective value for the Riks analysis with linear elements, which was 0.07. Hence, it can be concluded that using the explicit dynamic analysis procedure with the modelling type-3 provides the closest and most consistent agreement to the experimentally attained ultimate resistance, whilst the plastic resistance is also well-predicted, albeit slightly lower on average compared to the Riks analysis with 3 quadratic elements through the flange thickness. Bearing in mind the significant savings in computational cost associated with using explicit dynamic analysis, this analysis type is adopted in subsequent numerical studies throughout this project.

Table 7: Comparison of explicit dynamic procedure and static Riks analysis procedure.

	Type-3		
	3 elements through flange thickness		
	Linear	Quadratic	Explicit
	$F_{u,FEM}/ F_{u,Exp}$	$F_{u, FEM}/ F_{u,Exp}$	$F_{u, FEM}/ F_{u,Exp}$
Mean	1.00	1.01	1.00
COV	0.07	0.06	0.06

3.4 Through thickness stress distribution

An important numerical result that cannot be obtained experimentally is the distribution of stresses throughout the depth of the T-stub flange at the attainment of the plastic resistance F_{pl} as well as at the ultimate resistance F_u. This stress distribution through the thickness in conjunction with the corresponding bolt force can be utilised to determine the failure mode of the T-stub as demonstrated by Yuan et al. [38]. The stress distribution curves through the thickness were obtained for the thinnest and thickest flange thickness of the single and double bolt rows for each material grades considered (i.e. a total of 8 models) and are shown in Fig. 4. The stress distribution through the flange thickness is reported at three cross-sections along the length of the T-stubs, at the end of the fillet weld as shown in the relevant figures. The selected locations include the location of the bolt, middle of the T-stub and the end of the T-stub. The reported normal stresses have been normalised by the longitudinal nominal yield stress $\sigma_{0.2}$ and are plotted on the x-axis against the through thickness locations at which they occur, which are plotted on the y-axis. For each of the three locations along the length of the T-stub sections where the stress values are reported, two load levels were considered, namely the load corresponding to the plastic resistance of the T-stub $F_{pl, FE}$ and the ultimate load $F_{u, FE}$ with the stress distribution curves are denoted with solid and dotted lines, respectively.

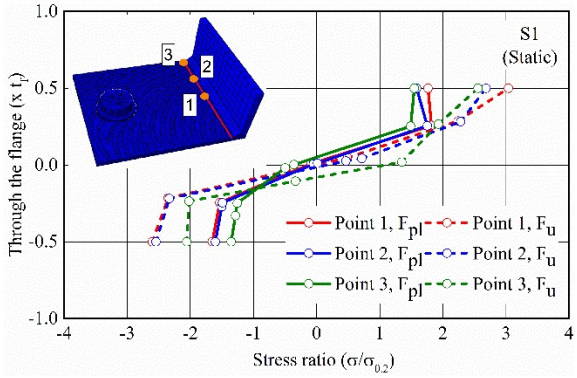

a) S1 Static Riks with quadratic mesh

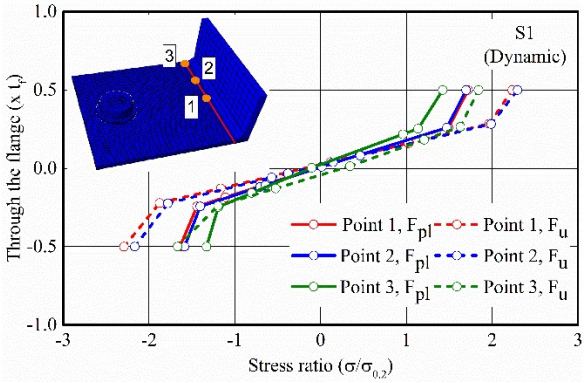

b) S1 Dynamic explicit

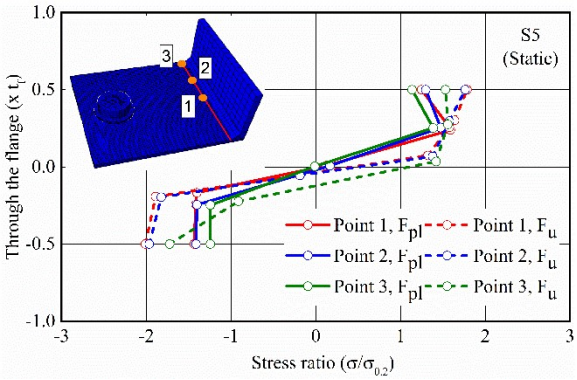

c) S5 Static Riks with quadratic mesh

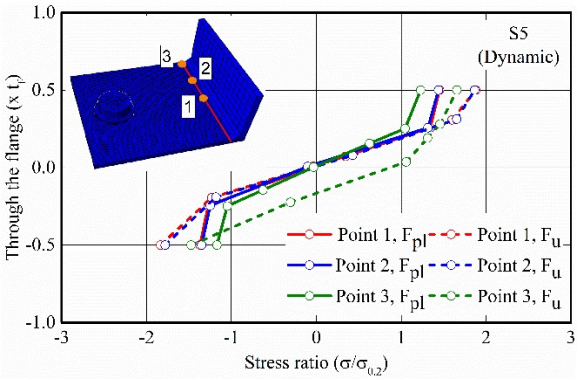

d) S5 Dynamic explicit

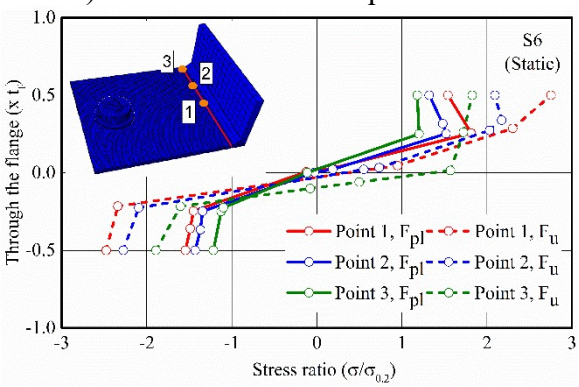

e) S6 Static Riks with quadratic mesh

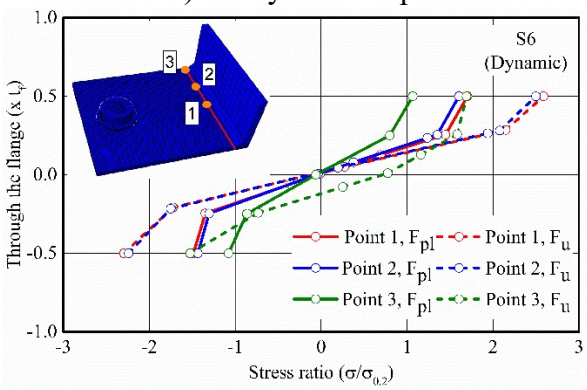

f) S6 Dynamic explicit

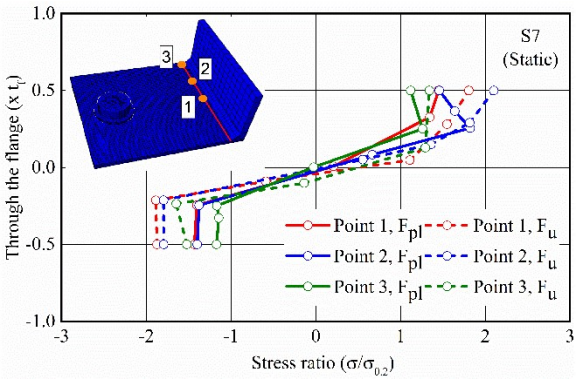

g) S7 Static Riks with quadratic mesh

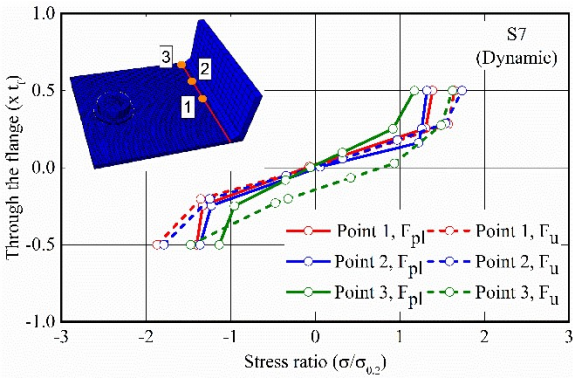

h) S7 Dynamic explicit

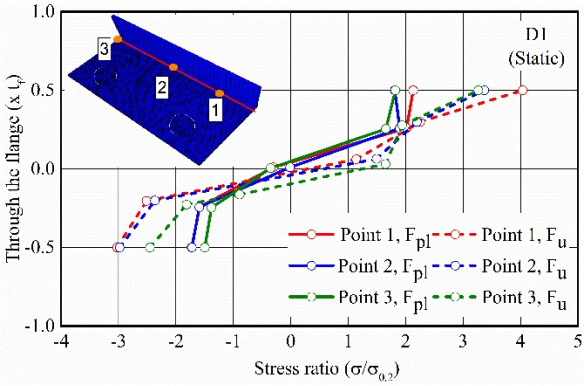

i) D1 Static Riks with quadratic mesh

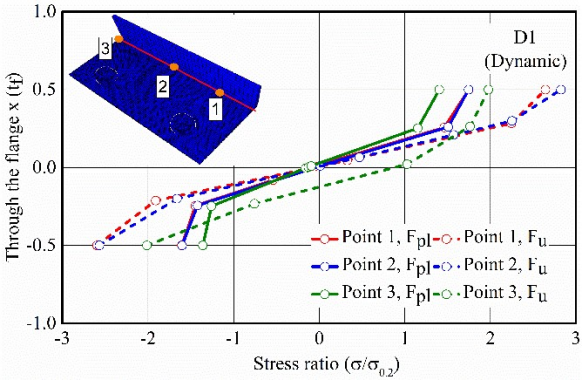

j) D1 Dynamic explicit

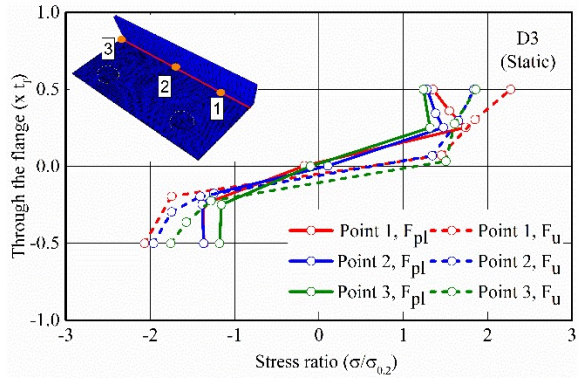

k) D3 Static Riks with quadratic mesh

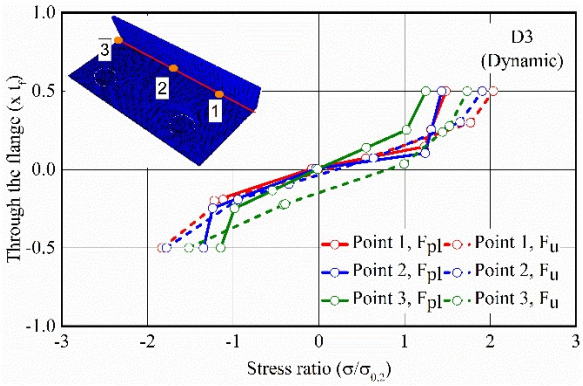

l) D3 Dynamic explicit

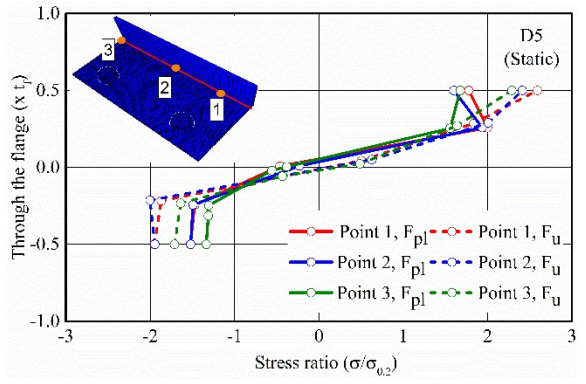

m) D5 Static Riks with quadratic mesh

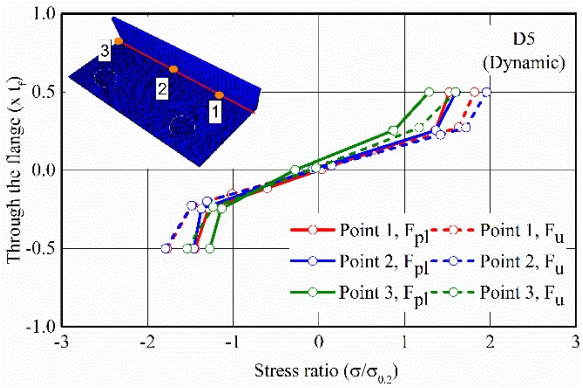

n) D5 Dynamic explicit

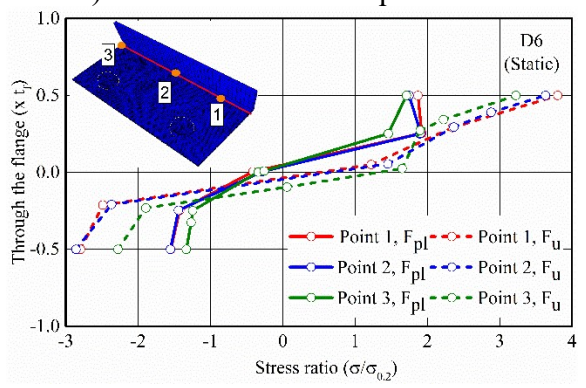

o) D6 Static Riks with quadratic mesh

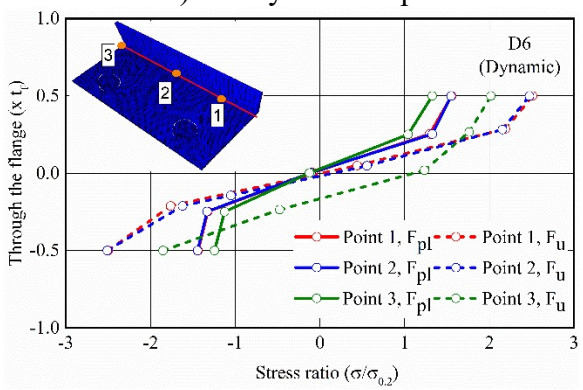

p) D6 Dynamic explicit

Fig. 4. Comparison of the stress distribution through the flange thickness for explicit dynamic and static analysis.

EN 1993-1-8 [1] assumes that the strength corresponding to Type-1 failure mode is obtained based on rigid plastic analysis in which rigid plastic material response is considered. This assumption is suitable for materials with a well-defined yield plateau, however for stainless steels, which exhibit a gradual loss of stiffness and significant strain hardening, this assumption becomes questionable. Hence, the attainment of stress distribution through the flange thickness at the load level which corresponds to the plastic resistance of the T-stub can provide valuable insight into the true stress-distribution at plastic resistance, which can be compared to the assumed one. In Fig. 4, it can be observed, that stress distribution in all locations are symmetric for all models. In all models, the T-stub section at the bolt location experiences higher stress values (red curves) compared to the other sections, whilst the lowest stress values were observed at the free ends of the T-stubs (green curves) with the intermediate locations (blue curves) being in-between depending on the bolt arrangement. The stress distributions obtained from the static Riks and dynamic explicit procedures at the attainment of the plastic resistance are very similar. Moreover, at the ultimate load level the stress distributions slightly differ and the normalised stress ratios are marginally larger for the static Riks analysis. Overall, it is concluded that the dynamic explicit analysis procedure can accurately simulate the stress distribution through the flange thickness and qualitatively similar results are obtained regardless of the employed type of analysis.

4. Parametric study

4.1 FE modelling and assumptions

In this parametric study, austenitic, duplex and ferritic stainless steel material grades were considered. Four different flange thickness were considered , namely 6, 9, 12 and 15 mm, three different m values such as 50, 65 and 80 mm and two different bolt diameter 12 and 16 mm were utilised. Additionally, the aspect ratio for the T-stub flanges was considered as 0.5. A total

of 72 different combinations of geometric configurations and material properties were considered, with all geometric dimensions and material properties reported in Tables 8 and 9, respectively. The modelling assumptions are identical to the ones utilised in the validation of the models discussed in section 2.1.

Table 8: Geometric dimensions of the specimens for the parametric study (units are in mm).

Material	Bolt	$t_f = t_w$	Width	m	n	d_b	h_f
Austenitic	A4-80	6	$b=b_f/2$	50	50	12	6
Duplex		9		65		16	
Ferritic		12		80			
		15					

Table 9: Material properties considered in the parametric study.

Stainless steel plates and bolts	Plate thickness or nominal bolt diameter (mm)	v	E_0 (MPa)	$\sigma_{0.01}$ (MPa)	$\sigma_{0.2}$ (MPa)	$\sigma_{1.0}$ (MPa)	σ_u (MPa)	ε_u (%)	ε_f (%)	n
EN 1.4301	11.85	0.258	182800	184.7	280.4	319.1	719.6	-	57.7	7.2
EN 1.4462	12.58	0.226	184000	227.8	464.6	552.8	705.3	23.3	37.4	4.2
Ferritic [45]	-	-	220000	-	320	-	480	0.16	-	17.2
A4-80	12	-	184500	271.5	553.9	710.4	794.0	5.9	29.7	4.2
A4-80	16	-	175300	300.7	524.4	682.3	765.4	9.8	33.4	5.4

The material properties of the parametric study for austenitic and duplex T-stubs, were adopted from Table 2 which correspond to the EN 1.4301 grade with 11.85 mm thickness and EN 1.4462 with 12.58 mm thickness, respectively. Likewise, the material characteristics of A4-80 bolts were selected according to Table 2. In addition, the material properties of the ferritic stainless steel T-stub were adopted from the study conducted by Afshan et al. [45] for hot-rolled sections.

4.2 Results and discussion

The results of the parametric study are reported in Table 10. The ultimate force, ultimate displacement and plastic strength were determined based on the numerical study. The stress distributions through the flange thickness were extracted for one representative T-stub failing in mode 1 and 2 for each of the three stainless steel material grades considered, as illustrated in

Fig. 5. The main observations regarding the symmetry of the stress distribution at F_{pl} and its progressive transition to an unsymmetrical one with pronounced membrane effects previously discussed can also be observed in Fig. 5. As expected the austenitic T-stub reaches higher stresses compared to its nominal yield strength than its ferritic and duplex counterparts due to the more pronounced strain-hardening inherent in the material response.

Table 10: Summary of the parametric numerical results stainless steel bolted T-stubs.

#	t_f (mm)	m (mm)	n (mm)	b_f (mm)	b (mm)	d_b (mm)	Austenitic			Duplex			Ferritic		
							$F_{u,FE}$ (KN)	$F_{pl,FE}$ (KN)	Δ_u (mm)	$F_{u,FE}$ (KN)	$F_{pl,FE}$ (KN)	Δ_u (mm)	$F_{u,FE}$ (KN)	$F_{pl,FE}$ (KN)	Δ_u (mm)
1	6	50	50	215.6	107.8	12	91.6	27.0	30.9	101.6	44.5	29.5	94.6	33.5	35.9
2	6	50	50	215.6	107.8	16	113.8	28.0	35.4	177.8	47.0	45.0	116.6	35.5	40.5
3	6	65	50	245.6	122.8	12	82.0	19.0	35.4	92.9	37.0	33.3	86.7	28.5	39.8
4	6	65	50	245.6	122.8	16	107.9	26.0	43.5	156.8	38.5	47.5	111.0	31.0	47.8
5	6	80	50	275.6	137.8	12	74.8	19.0	38.8	85.2	32.0	38.3	80.4	23.0	43.0
6	6	80	50	275.6	137.8	16	95.3	22.5	38.8	140.2	32.0	53.4	101.8	25.5	46.7
7	9	50	50	218.6	109.3	12	106.8	60.0	21.1	111.5	79.0	12.6	106.8	71.0	21.1
8	9	50	50	218.6	109.3	16	184.0	66.0	36.8	186.1	106.5	29.7	184.6	81.0	39.0
9	9	65	50	248.6	124.3	12	98.4	51.0	25.2	102.4	70.0	16.8	98.4	60.0	25.2
10	9	65	50	248.6	124.3	16	167.7	55.0	39.9	175.0	88.0	37.5	169.3	68.0	44.0
11	9	80	50	278.6	139.3	12	92.1	42.0	30.1	95.8	65.0	21.2	92.1	56.0	30.1
12	9	80	50	278.6	139.3	16	156.0	46.0	45.9	162.7	80.0	41.9	223.1	59.5	45.0
13	12	50	50	221.6	110.8	12	122.2	82.0	13.4	139.4	90.0	15.9	122.2	88.0	13.4
14	12	50	50	221.6	110.8	16	192.0	122.0	28.0	202.2	150.5	19.4	192.0	136.0	28.0
15	12	65	50	251.6	125.8	12	111.8	73.0	16.3	126.5	83.5	18.5	111.8	85.0	16.3
16	12	65	50	251.6	125.8	16	179.2	103.0	34.5	182.8	135.0	25.0	179.2	119.5	34.5
17	12	80	50	281.6	140.8	12	103.5	66.5	18.0	117.9	73.5	21.3	103.5	78.0	18.0
18	12	80	50	281.6	140.8	16	168.5	89.0	39.3	170.0	123.0	28.8	168.5	102.0	39.3
19	15	50	50	224.6	112.3	12	146.0	100.0	14.3	154.0	113.0	10.3	146.0	111.0	14.3
20	15	50	50	224.6	112.3	16	211.6	150.5	19.7	235.5	172.5	20.4	211.6	159.0	19.7
21	15	65	50	254.6	127.3	12	135.2	88.0	16.4	156.6	98.0	16.8	135.2	102.0	16.4
22	15	65	50	254.6	127.3	16	194.1	135.0	22.9	216.7	158.0	23.1	194.1	148.5	23.0
23	15	80	50	284.6	142.3	12	126.4	81.0	18.5	149.8	89.0	21.3	126.4	97.5	18.5
24	15	80	50	284.6	142.3	16	180.8	120.0	26.1	201.8	147.0	26.9	180.8	133.0	26.1

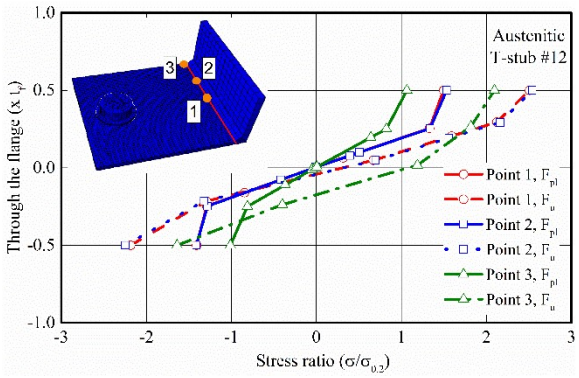

a) Austenitic Mode 1

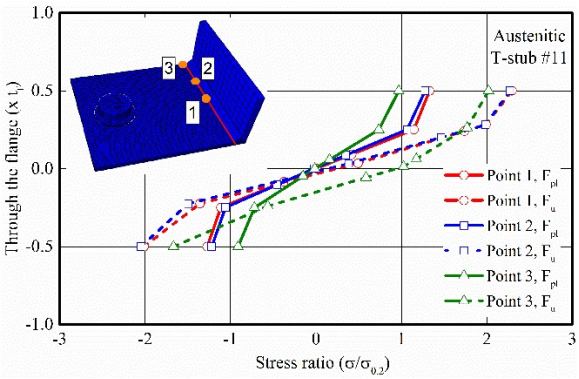

b) Austenitic Mode 2

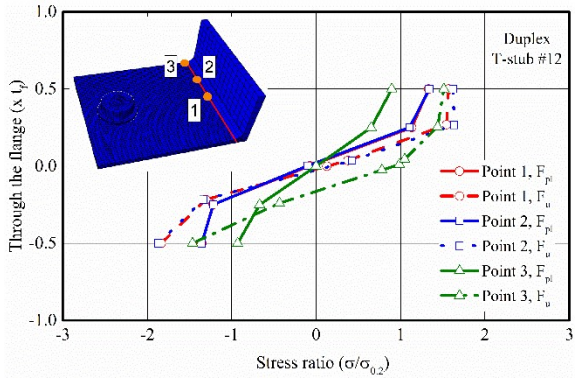

c) Duplex Mode 1

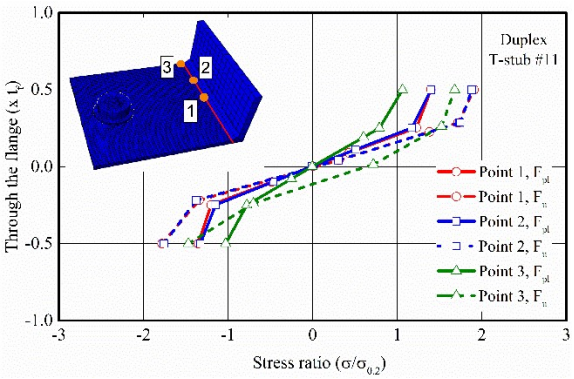

d) Duplex Mode 2

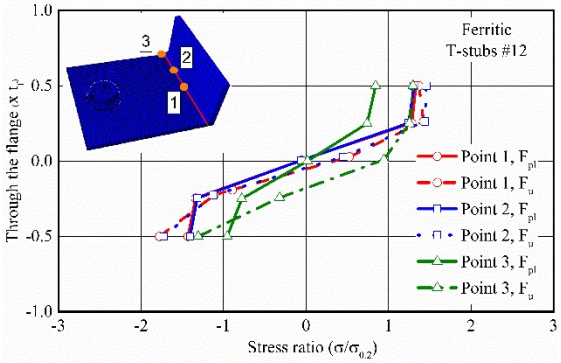

e) Ferritic Mode 1

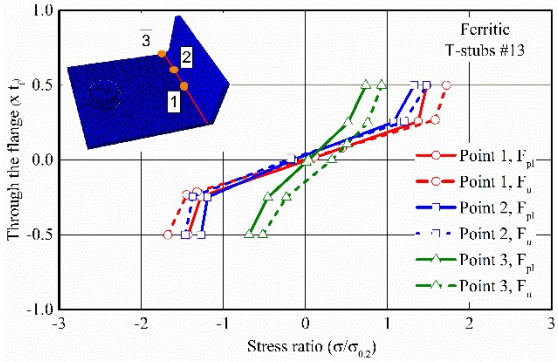

f) Ferritic Mode 2

Fig. 5. Stress distribution through the flange thickness.

5. Design recommendations

5.1 EN 1993-1-8 design provisions for T-stubs

The expressions to predict the plastic resistances corresponding to the three failure modes identified in EN 1993-1-8 [1] for stainless steel bolted T-stubs are given by Equations 1-3, where all symbols are defined in EN 1993-1-8 [1].

Type-1 $$F_{1,Rd} = \frac{(8n - 2e_w)M_{f,1,Rd}}{2mn - e_w(m+n)} \qquad M_{f,1,Rd} = 0.25 l_{eff,1} t_f^2 f_y / \gamma_{M0} \qquad (1)$$

Type-2 $$F_{2,Rd} = \frac{2M_{f,2,Rd} + n\Sigma F_{t,Rd}}{m+n} \qquad M_{f,2,Rd} = 0.25 l_{eff,2} t_f^2 f_y / \gamma_{M0} \qquad (2)$$

Type-3 $$F_{3,Rd} = \Sigma F_{t,Rd} \qquad (3)$$

Furthermore, the theoretical relationship between the thickness squared (t_f^2) and plastic resistance of T-stubs is depicted in Fig. 6. It can be observed that the resistance F_{pl} is proportional to t_f^2 for type 1 and type 2 failure modes, albeit with a different factor of proportionality, however type-3 failure mechanism is not affected by any change in thickness since it only involves bolt failure.

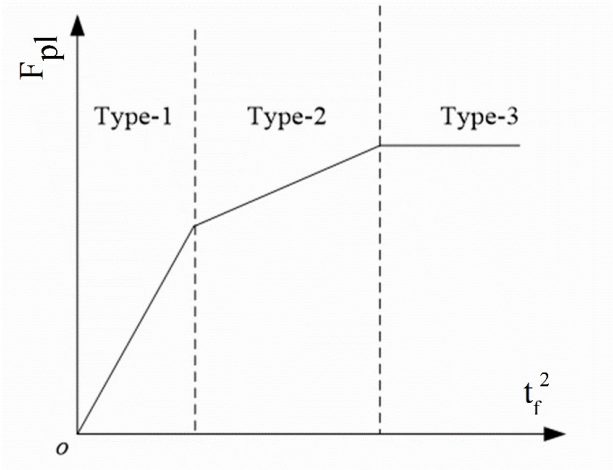

Fig. 6. Theoretical relationship between F_{pl} and t_f^2 provided in EN 1993-1-8.

5.2 Effect of flange thickness on plastic resistance

The relationship between the thickness squared (t_f^2) and plastic resistance of T-stubs which were obtained by parametric study utilising developed FE model is depicted in Fig. 7. It can be observed that the obtained results for all three types of stainless steels are consistent with the theoretical model provided in EN 1993-1-8 [1] (Fig. 7). As the thickness squared increases the correlation between the plastic resistance force and thickness squared becomes lower which

means T-stubs exhibited mostly mode 1 and mode 2 failure mechanisms. Moreover, the influence of bolt diameter on the plastic resistance is significant for all three stainless steel grades for the two failure modes involving bolt failure (type 2 and type 3).

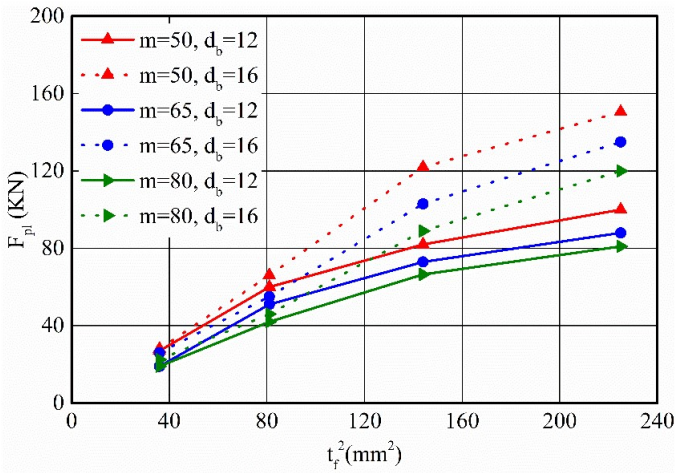

(a) Austenitic T-stubs

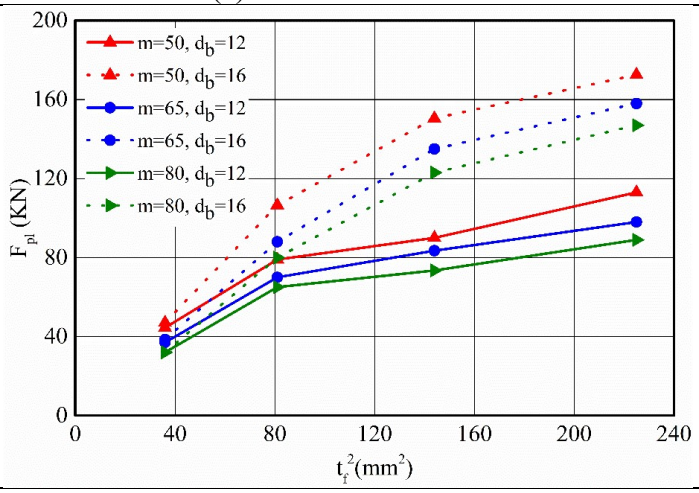

(b) Duplex T-stubs

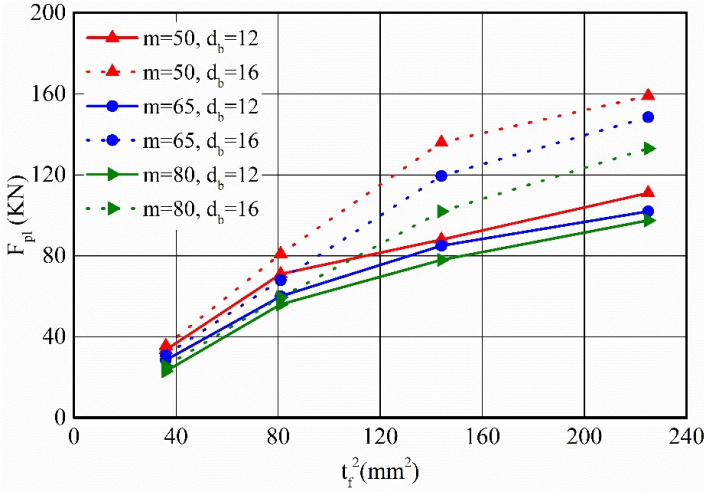

(c) Ferritic T-stubs

Fig. 7. Effect of flange thickness on plastic resistance.

5.3 Assessment of plastic resistance predictions

The parametric study results are compared with the plastic resistance predictions based on EN 1993-1-8 [1] and mean value of the ratios between the predicted plastic forces based on the design provisions and the numerically obtained ones are given in Table 11.

The average values of the ratios between the plastic strength predictions of EN 1993-1-8 [1] and parametric FE analysis were obtained as 0.92, 0.98 and 0.86 for austenitic, duplex and ferritic stainless steel grade T-stubs, respectively. The failure modes of the T-stubs were determined based on the EN 1993-1-8 [1] resistance predictions. The lowest predicted resistance of all three failure modes govern the failure of the specimens. An important conclusion that can be drawn is that the plastic resistances of the T-stubs which have Type 1 failure mode were overpredicted, for the ones with failure mode 2 the plastic resistances were slightly overpredicted, and for the T-stubs with failure mode 3 the plastic resistances were obtained with a good agreement. This pattern was observed for all three types of stainless steel grade as can be seen in Table 11.

Table 11 Comparison of plastic resistances obtained by EN 1993-1-8 [1] and FE models.

		$F_{pl\ EN} / F_{pl\ FEM}$	$F_{pl\ EN} / F_{pl\ FEM}$	$F_{pl\ EN} / F_{pl\ FEM}$
		Austenitic	Duplex	Ferritic
Overall	Mean	0.92	0.98	0.86
	COV	0.09	0.09	0.07
Mode 1	Mean	0.83	0.90	0.81
	COV	0.04	0.07	0.06
Mode 2	Mean	0.90	0.94	0.85
	COV	0.09	0.08	0.03
Mode 3	Mean	0.99	1.03	0.91
	COV	0.03	0.07	0.03

In Fig. 8 the ratio of the plastic resistances which are predicted by EN 1993-1-8 [1] and obtained by generated FE model is plotted against the square of the flange thickness of the T-stubs to provide much better representation for the validation of developed FE model. The scatter of the

values for failure mode 1 is much wider and implies an overprediction of the plastic resistances. Likewise the distribution of the scatter data is observed as spread out for failure mode 2 and more concentrated scatter is obtained when the T-stubs failed in failure mode 3.

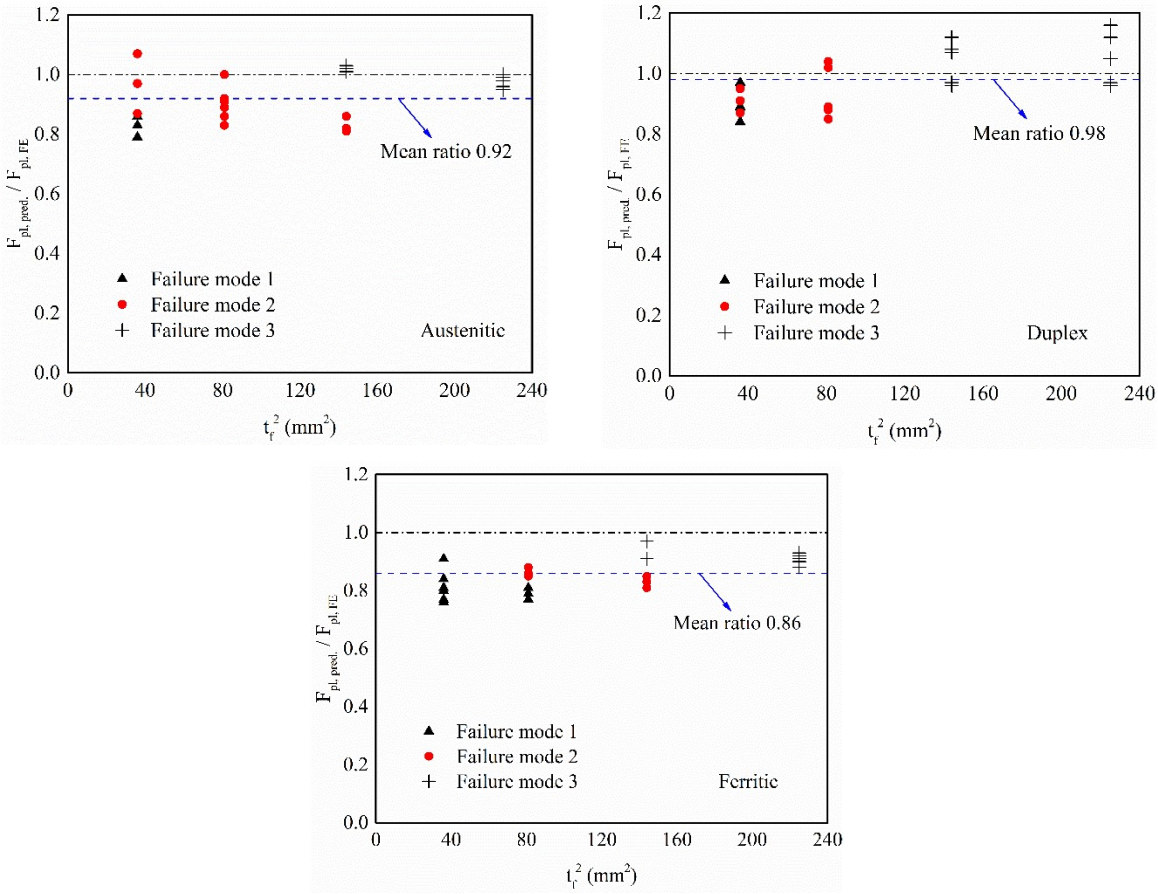

Fig. 8. The relationship between $F_{pl,pred.} / F_{pl,FE}$ and t_f^2.

6. Conclusions

An advanced FE model was developed to simulate the overall behaviour of stainless steel bolted T-stubs in tension considering failure modes and fracture mechanism of stainless steel bolts. The developed FE model was validated against published test results on experimental behaviour of stainless steel bolted T-stubs in tension which was reported recently by Yuan et al. [30]. Recommendations have been made for the best modelling approach regarding modelling of bolt and weld geometry. A parametric study was performed using single bolt row stainless steel T-stubs considering different geometric configurations and three material grades, representing

austenitic, ferritic and duplex stainless steel [45] to investigate the effect of plate thickness, material grade, bolt spacing and flange width on the plastic resistance, ultimate capacity and ductility of joints as well as overall response. In the light of obtained results the design provisions of EN 1993-1-8 were assessed. Following conclusions can be drawn in line with the results reported herein.

Modelling of the bolt as smooth cylindrical with effective cross-section area can predict the plastic force and ultimate force of the T-stubs more accurately rather than the FE models in which the unthreaded diameter of the bolt is taken as the outer diameter, and a hole is drilled in the cylinder to provide the nominal stress area. Including the welds between the web and flange into the FE models provides more accurate force and displacement predictions for bolted T-stubs in tension.

It can be concluded that, using quadratic elements instead of linear elements has no significant effect on the ultimate forces and it only affects the trend of the force displacement curves after the attainment of the ultimate load. The FE model with quadratic elements predicts the plastic force values more accurately and consistently. Additionally, the type-3 numerical model exhibits better results in terms of ultimate force predictions and it provides simpler solution and low computational cost. On the other hand, the type-4 numerical model shows better results in terms of ultimate displacement values.

The mean values of $F_{u, FEM}/ F_{u, Exp}$ was procured as 1.00 with explicit dynamic procedure which is equal to static Riks procedure with linear mesh. Furthermore, in line with the comparison of stress distribution through the flange thickness, it was reported that the dynamic explicit analysis procedure can simulate the stress distributions through the flange thickness accurately and agrees well with the static Riks analysis procedure.

In the parametric analysis, the average values of the ratios between the plastic strength predictions of EN 1993-1-8 and FE analysis were obtained as 0.92, 0.98 and 0.86 for the bolted T-stubs made of austenitic, duplex and ferritic stainless steel grade, respectively. It can be concluded that the plastic resistance predictions provided by the developed FE model agree well with the predictions by EN 1993-1-8 for austenitic and duplex stainless steel bolted T-stubs and the FE model slightly overpredicts the plastic resistance of the T-stubs made of ferritic stainless steel. Additionally, it was observed that the plastic resistances were overpredicted for the T-stubs failing particularly in type 1 and type 2 failure modes for all stainless steel grades. The predictions were obtained more accurately when the type-3 failure mode is obtained. The overall behaviour of stainless steel bolted T-stubs in tension can be simulated accurately with developed FE model.

Based on the attainment of symmetric stress distributions through the flange thickness in parametric analysis, the main load carrying mechanism up to the attainment of the plastic resistance of the section is bending. However, it was observed that at the attainment of ultimate force, the stress distribution exhibits a clear asymmetry which means the T-stubs are no longer under bending effect only, they are carrying simultaneously bending moment and tension due to the membrane actions which is mainly caused by thinner flange thickness.

REFERENCES

[1] EN 1993-1-8:2005/AC:2009, Eurocode 3: Design of steel structures - Part 1-8: Design of joints.

[2] Zoetemeijer P. A Design Method for the Tension Side of Statically Loaded, Bolted Beam-to-Column Connections. HERON 20 1 1974 1974.

[3] Packer JA, Morris LJ. A limit state design method for the tension region of bolted beam-column connections. Struct Eng 1977;5:446–58.

[4] Yee YL, Melchers RE. Moment-Rotation Curves for Bolted Connections. J Struct Eng-Asce 1986;112:615–35.

[5] Faella C, Piluso V, Rizzano G. Reliability of Eurocode-3 Procedures for Predicting Beam-to-Column Joint Behaviour. Istanbul: Bogazici University Bebek; 1995.

[6] Faella C, Piluso V, Rizzano G. Structural steel semirigid connections : theory, design, and software. Boca Raton ; London : CRC Press; 2000.

[7] Jaspart JP, Maquoi R. Effect of bolt preloading on joint behaviour. Proc Steel Struct Eurosteel 95 Kounadis Ed Balkema Rotterdam Neth 1995:219–26.

[8] Faella C, Piluso V, Rizzano G. Structural steel semirigid connections : theory, design, and software. Boca Raton ; London : CRC Press; 2000.

[9] Coelho AMG, Bijlaard FSK, Gresnigt N, da Silva LS. Experimental assessment of the behaviour of bolted T-stub connections made up of welded plates. J Constr Steel Res 2004;60:269–311.

[10] Piluso V, Faella C, Rizzano G. Ultimate behavior of bolted T-stubs. II: Model validation. J Struct Eng-ASCE 2001;127:694–704.

[11] Swanson JA, Leon RT. Bolted steel connections: Tests on T-stub components. J Struct Eng-ASCE 2000;126:50–6.

[12] Piluso V, Faella C, Rizzano G. Ultimate behavior of bolted T-stubs. I: Theoretical model. J Struct Eng-ASCE 2001;127:686–93.

[13] Beg D, Zupančič E, Vayas I. On the rotation capacity of moment connections. J Constr Steel Res 2004;60:601–20.

[14] Coelho AMG. Characterization of the ductility of bolted end plate beam-to-column steel connections. PhD Thesis Universidade Coimbra 2004.

[15] Swanson JA, Leon RT. Stiffness Modeling of Bolted T-Stub Connection Components. J Struct Eng 2001;127:498–505.

[16] Coelho AMG, da Silva LS, Bijlaard FSK. Ductility analysis of bolted extended end plate beam-to-column connections in the framework of the component method. Steel Compos Struct 2006;6:33–53.

[17] O.S. Bursi, J.P. Jaspart, Benchmarks for finite element modelling of bolted steel connections, J. Constr. Steel Res. 43 (1997) 17–42.

[18] Zajdel, M. _1997_. "Numerical analysis of bolted tee-stub connections." TNO-Rep. No. 97-CON-R-1123.

[19] E.S. Mistakids, C.C. Baniotopoulos, C.D. Bisbos, P.D. Panagiotopoulos, Steel T-stub connections under static loading: an effective 2-D numerical model, J. Constr. Steel Res. 44 (1997) 51–67.

[20] J.A. Swanson, D.S. Kokan, R.T. Leon, Advanced finite element modelling of bolted T-stub connection components, J. Constr. Steel Res. 58 (2002) 1015–1031.

[21] C.J. Gantes, M.E. Lemonis, Influence of equivalent bolt length in finite element modelling of T-stub steel connections, Comput. Struct. 81 (2003) 595–604.

[22] A.M.G. Coelho, L.S.D. Silva, F.S.K. Bijlaard, Finite-element modelling of the nonlinear behaviour of bolted T-stub connections, J. Struct. Eng. 132 (2006) 918–928.

[23] Coelho AMG, da Silva LS, Bijlaard FSK. Ductility analysis of bolted extended end plate beam-to-column connections in the framework of the component method. Steel Compos Struct 2006;6:33–53. doi:10.12989/scs.2006.6.1.033.

[24] A.B. Francavilla, M. Latour, V. Piluso, G. Rizzano, Simplified finite element analysis of bolted T-stub connection components, Eng. Struct. 100 (2015) 656–664.

[25] J.F. Ceniceros, A.S. Garcia, F.A. Torres, F.J.M.D.A. Pison. A numerical-informational approach for characterising the ductile behaviour of the T-stub component. Part 1: refined finite element model and test validation, Eng. Struct. 82 (2015) 236–248.

[26] J.F. Ceniceros, A.S. Garcia, F.A. Torres, F.J.M.D.A. Pison. A numerical-informational approach for characterising the ductile behaviour of the T-stub component. Part 2: parsimonious soft-computing-based metamodel, Eng. Struct. 82 (2015) 249–260.

[27] Kong Z, Kim S-E. Numerical estimation for initial stiffness and ultimate moment of T-stub connections. Journal of Constructional Steel Research 2018;141:118–31.

[28] Gödrich L, Wald F, Kabeláč J, Kuříková M. Design finite element model of a bolted T-stub connection component. Journal of Constructional Steel Research 2019;157:198–206.

[29] Bouchair A, Averseng J, Abidelah A. Analysis of the behaviour of stainless steel bolted connections. J Constr Steel Res 2008;64:1264–74.

[30] Yuan HX, Hu S, Du XX, Yang L, Cheng XY, Theofanous M. Experimental behaviour of stainless steel bolted T-stub connections under monotonic loading. J Constr Steel Res 2019; 152:213–24.

[31] Elflah M, Theofanous M, Dirar S, Yuan HX. Behaviour of stainless steel beam-tocolumn joints—Part 1: Experimental investigation. J Constr Steel Res 2019;152:183-93.

[32] Elflah M, Theofanous M, Dirar S. Behaviour of stainless steel beam-to-column joints—Part 2: Numerical modelling parametric study. J Constr Steel Res 2019;152:194-212.

[33] Elflah M, Theofanous M, Dirar S, Yuan H. Structural behaviour of stainless steel beam-to-tubular column joints. Engineering Structures 2019;184:158–75. https://doi.org/10.1016/j.engstruct.2019.01.073.

[34] Wang, J., Uy, B. and Li, D. (2019). Behaviour of large fabricated stainless steel beam-to-tubular column joints with extended endplates", Steel Compos. Struct., Int. J., 32(1), 141-156.

[35] Bu, Y., Wang, Y. and Zhao, Y. (2019) Study of stainless steel bolted extended end-plate joints under seismic loading. Thin-Walled Structures, 144: 106255.

[36] Song, Y. & Uy, B. and Wang, J. (2019). Numerical analysis of stainless steel-concrete composite beam-to-column joints with bolted flush endplates. Steel and Composite Structures. 33. 975-994. 10.12989/scs.2019.33.1.975.

[37] Gao, J.D., Yuan, H.X., Du, X.X., Hu, X.B., Theofanous, M., 2020. Structural behaviour of stainless steel double extended end-plate beam-to-column joints under monotonic loading. Thin-Walled Structures 151, 106743.

[38] Yuan HX, Gao JD, Theofanous M, Yang L, Schafer BW. Initial stiffness and plastic resistance of bolted stainless steel T-stubs in tension. Journal of Constructional Steel Research 2020;173:106239.

[39] Yapici O, Theofanous M, Dirar S, Yuan H. Behaviour of Ferritic Stainless Steel Bolted T-stubs Under Tension-Part 1: Experimental Investigations. Ce/Papers 2021;4:866–75. https://doi.org/10.1002/cepa.1372.

[40] Yapici O, Theofanous M, Dirar S, Yuan H. Behaviour of Ferritic Stainless Steel Bolted T-stubs Under Tension-Part 2: Numerical Investigations. Ce/Papers 2021;4:876–85. https://doi.org/10.1002/cepa.1373.

[41] Yapici O, Theofanous M, Yuan H, Skalomenos K, Dirar S. Experimental study of ferritic stainless steel bolted T-stubs under monotonic loading. Journal of Constructional Steel Research 2021;183:106761. https://doi.org/10.1016/j.jcsr.2021.106761.

[42] Yapici O (2021). Ultimate response of stainless steel bolted connections, The University of Birmingham, PhD dissertation.

[43] ABAQUS Theory Manual, ver. 6.13. Dassault Systèmes Simulia Corp Provid RI USA 2013.

[44] Quach W.M., Teng J.G., Chung K.F. Three-Stage Full-Range Stress-Strain Model for Stainless Steel. Journal of Structural Engineering 2008; 134: 1518-1527.

[45] Afshan S, Zhao O, Gardner L. Standardised material properties for numerical parametric studies of stainless steel structures and buckling curves for tubular columns. Journal of Constructional Steel Research 2019; 152:2–11.